Applied Physics Letters

Band alignment at β-$(Al_xGa_{1-x})_2O_3$/β-Ga_2O_3 (100) interface fabricated by pulsed-laser deposition

Cite as: Appl. Phys. Lett. **112**, 232103 (2018); https://doi.org/10.1063/1.5027005
Submitted: 26 February 2018 . Accepted: 20 May 2018 . Published Online: 07 June 2018

Ryo Wakabayashi, Mai Hattori, Kohei Yoshimatsu, Koji Horiba, Hiroshi Kumigashira, and Akira Ohtomo

Band alignment at β-$(Al_xGa_{1-x})_2O_3$/β-Ga_2O_3 (100) interface fabricated by pulsed-laser deposition

Ryo Wakabayashi,[1,a)] Mai Hattori,[1] Kohei Yoshimatsu,[1] Koji Horiba,[2,3] Hiroshi Kumigashira,[2,3] and Akira Ohtomo[1,3]
[1]*Department of Chemical Science and Engineering, Tokyo Institute of Technology, 2-12-1 Ookayama, Meguro-ku, Tokyo 152-8552, Japan*
[2]*Photon Factory, Institute of Materials Structure Science, High Energy Accelerator Research Organization, Tsukuba, Ibaraki 305-0801, Japan*
[3]*Materials Research Center for Element Strategy (MCES), Tokyo Institute of Technology, Midori-ku, Yokohama 226-8503, Japan*

(Received 26 February 2018; accepted 20 May 2018; published online 7 June 2018)

High-quality β-$(Al_xGa_{1-x})_2O_3$ ($x = 0$–0.37) films were epitaxially grown on β-Ga_2O_3 (100) substrates by oxygen-radical-assisted pulsed-laser deposition with repeating alternate ablation of single crystals of β-Ga_2O_3 and α-Al_2O_3. The bandgap was tuned from 4.55 ± 0.01 eV ($x = 0$) to 5.20 ± 0.02 eV ($x = 0.37$), where bowing behavior was observed. The band alignment at the β-$(Al_xGa_{1-x})_2O_3$/β-Ga_2O_3 interfaces was found to be type-I with conduction- and valence-band offsets of 0.52 ± 0.08 eV (0.37 ± 0.08 eV) and 0.13 ± 0.07 eV (0.02 ± 0.07 eV) for $x = 0.37$ (0.27), respectively. The large conduction-band offsets are ascribed to the dominant contribution of the cation-site substitution to the conduction band. *Published by AIP Publishing.*
https://doi.org/10.1063/1.5027005

β-Ga_2O_3 is a wide-gap semiconductor attracting growing interest in recent years. β-Ga_2O_3 has a β-gallia structure, which is the most stable phase in polymorphs of α-, β-, γ-, δ-, and ε-phases.[1] Owing to its wide bandgap ($E_g = 4.4$–4.6 eV),[2,3] the breakdown electric field is expected to be as high as 8 MV/cm, which leads to substantially large Baliga's figure of merit over 4H-SiC and GaN.[4] The electron concentration (n) can be regulated in a range from 10^{16} to 10^{19} cm^{-3} by introducing oxygen vacancy and/or substituting Ga sites with Si, Ge, or Sn,[5–9] while highly insulating properties are realized by substituting with Fe.[10] Moreover, large and high-quality single crystals can be synthesized by melt growth methods such as the floating-zone, Czochralski, vertical Bridgman, and edge-defined film-fed growth, which are usable for practical applications.[11–14] These advantages are promising for power device applications such as high-power Schottky barrier diodes[15] and field-effect transistors (FETs).[16,17]

The E_g of β-Ga_2O_3 can be tuned in solid solutions, such as β-$(Al_xGa_{1-x})_2O_3$, enabling preparation of ideal potential barriers in a heterojunction field-effect transistor (HFET). The solubility limit of Al_2O_3 in the β-phase solid solution is reported to be $x \sim 0.7$, corresponding to E_g as wide as 6.1 eV.[18] The demonstration of electron accumulation at β-$(Al_xGa_{1-x})_2O_3$/β-Ga_2O_3 interfaces[19] and transistor operations in modulation-doped β-$(Al_xGa_{1-x})_2O_3$/β-Ga_2O_3 FETs have been attempted.[9,20] Therefore, two-dimensional electron gas (2DEG) at the interface can be in principle realized to achieve high-mobility and high-frequency operation of HFETs.

Band offsets, namely, energy discontinuities of conduction-band minima (ΔE_C) and valence-band maxima (ΔE_V) between semiconductors and adjacent layers, are one of the most important parameters for designing heterojunction devices. In β-Ga_2O_3 based heterojunctions, there are several reports on the band offsets between insulating oxides/β-Ga_2O_3: $\Delta E_C = 1.9$ eV and $\Delta E_V = 0.5$ eV at γ-Al_2O_3/β-Ga_2O_3 and $\Delta E_C = 3.1$ eV and $\Delta E_V = 1.0$ eV at SiO_2/β-Ga_2O_3.[3,21] On the other hand, the experimental determination of band offsets at the β-$(Al_xGa_{1-x})_2O_3$/β-Ga_2O_3 interface has not been reported yet. For determination of band offsets, electron spectroscopies such as reflection electron energy loss spectroscopy (REELS) and X-ray photoemission spectroscopy (XPS) are used commonly,[3,21,22] where the band alignment is determined from E_g and core levels of each material and/or their interface. This method is particularly suitable to insulating samples such as γ-Al_2O_3, SiO_2, and undoped β-$(Al_xGa_{1-x})_2O_3$ grown on β-Ga_2O_3.

In this letter, we study β-$(Al_xGa_{1-x})_2O_3$ films grown on β-Ga_2O_3 (100) substrates to determine the band alignments from REELS and XPS measurements. Higher crystallinity and flatness of β-$(Al_xGa_{1-x})_2O_3$ ($x = 0$–0.37) films were realized using the repeating alternate target ablation technique in oxygen-radical-assisted pulsed-laser deposition (PLD). E_g increased from 4.55 ± 0.01 ($x = 0$) to 5.20 ± 0.02 eV ($x = 0.37$), and E_g as a function of x indicates the bowing behavior. Moreover, type-I band alignment with considerably large $\Delta E_C/\Delta E_V$ (4.0 at $x = 0.37$) was found.

β-Ga_2O_3 and β-$(Al_xGa_{1-x})_2O_3$ films were grown on n-type β-Ga_2O_3 (100) substrates (Tamura Corp.) by oxygen-radical-assisted PLD.[23] The size and thickness of the substrates were 5×10 mm^2 and 650 μm, respectively. The target materials used in this study were either single crystals of β-Ga_2O_3 and α-Al_2O_3 or a sintered $(Al_{0.2}Ga_{0.8})_2O_3$ tablet. Focused KrF excimer laser pulses (10 Hz and 0.5 J cm^{-2}) were introduced to the targets placed 5 cm away from the substrate surface. The growth temperature (T_g) was set at 500 °C (temperature of the SiC plate measured through the substrates using a pyrometer). The oxygen radicals were supplied from a RF plasma cell operated at 100 W with feeding

a)Electronic mail: wakabayashi.r.aa@m.titech.ac.jp

0.50 sccm O_2 gas (6N purity), corresponding to a constant pressure of 5×10^{-5} Torr in a vacuum chamber. All the β-$(Al_xGa_{1-x})_2O_3$ films were insulating.

The film thickness of β-Ga_2O_3 and β-$(Al_xGa_{1-x})_2O_3$ films was measured using a stylus profiler and X-ray reflectivity, respectively. The surface morphology was observed by scanning electron microscopy (SEM) and tapping mode atomic force microscopy (AFM). The epitaxial structure and crystallinity were investigated by X-ray diffraction (XRD) (Rigaku, SmartLab) with Cu Kα_1 radiation ($\lambda = 1.540562$ Å). The incident Cu Kα_1 X-ray was monochromatized by the Ge (220) 2-bounce monochromator. The composition of β-$(Al_xGa_{1-x})_2O_3$ films was determined by Auger electron spectroscopy (AES), where $(Al_{0.40}Ga_{0.60})_2O_3$ ceramics were used as a standard for calibration of the signal ratio of Al to Ga. REELS and XPS measurements were carried out at room temperature. The E_g values were estimated by REELS with an incident electron energy of 1 keV. XPS were performed using a VG-Scienta R3000 analyzer with a monochromatized Al Kα X-ray source (1486.6 eV), where the total energy resolution was 400 meV. C 1*s* core levels of the surface adsorbate (284.8 eV) were used to calibrate the binding energy.

We employed the repeating alternate target ablation technique for the growth of high-quality β-$(Al_xGa_{1-x})_2O_3$ films. In this technique, two targets, single crystals of β-Ga_2O_3 and α-Al_2O_3, were alternately ablated to deposit fractional monolayers within single cycles. Repeating a number of cycles with different ratios of numbers of laser pulses impinging each target, solid-solution films with various compositions were prepared.[24,25] In addition, the use of high-purity single crystals enabled us to grow high-purity β-$(Al_xGa_{1-x})_2O_3$ films. Figure 1 shows the out-of-plane XRD patterns and SEM images of 50-nm-thick β-$(Al_xGa_{1-x})_2O_3$ ($x \sim 0.2$) films grown with conventional laser ablation [continuous target ablation of sintered $(Al_{0.2}Ga_{0.8})_2O_3$] and the repeating alternate target ablation technique. Only β-$(Al_xGa_{1-x})_2O_3$ *h*00 reflections were observed for both films, indicating single-phase (100)-oriented films. The conventional laser ablation resulted in formation of dense and granular protrusions on the surface as observed in the SEM image [inset of Fig. 1(a)]. The protrusion density was found to increase when higher-x targets were used, while such a dense protrusion was not observed at all when single-crystal targets were used (not shown). These facts suggest that the sintered materials are the origin of protrusion formation, presumably arising from direct ejection of grains from the porous surface of the sintered targets.[26] In contrast, when the repeating alternate target ablation technique was employed, the clear Laue fringes were observed in the out-of-plane XRD pattern, indicating the sharp interface and the flat surface. Moreover, the protrusion formation was drastically suppressed [inset of Fig. 1(b)]. The full-width at half-maximum of the ω rocking curve ($\Delta\omega$) for the β-$(Al_xGa_{1-x})_2O_3$ 600 reflection grown with continuous and alternative laser ablation was 367 and 295 arc sec, respectively. The root mean square (RMS) roughness of an area of 5×5 μm^2 in AFM was 0.5 and 0.2 nm for the films grown with continuous and alternative laser ablation, respectively. See supplementary material of the AFM images (Fig. S1). The roughness of β-$(Al_xGa_{1-x})_2O_3$ films would affect data accuracy of surface-sensitive spectroscopies, and it would be increasingly difficult to access the electronic states intrinsic to the interface if dense protrusions exist. The use of single crystalline targets with the repeating alternate target ablation technique, therefore, is essential to prepare ideal samples for the investigation with the electron spectroscopies. For the above reasons, subsequent β-$(Al_xGa_{1-x})_2O_3$ films were grown with the repeating alternate target ablation technique.

β-$(Al_xGa_{1-x})_2O_3$ films with various Al contents were grown by the same technique. The RMS roughness of the films was found to be constant around 0.2 nm. Figure 2(a) shows the out-of-plane XRD patterns of 50-nm-thick β-$(Al_xGa_{1-x})_2O_3$ films. The peaks for the films were assigned to be the 400, 600, and 800 reflections of β-$(Al_xGa_{1-x})_2O_3$. The $\Delta\omega$ of the films with $x = 0.08$, 0.19, 0.28, and 0.37 was 324, 295, 544, and 713 arc sec, respectively. The increase in $\Delta\omega$ with x can be attributed to increasing lattice mismatch.

Figure 2(b) shows the reciprocal space map around the 912 reflection of the β-$(Al_{0.28}Ga_{0.72})_2O_3$ film on the β-Ga_2O_3 (100) substrate. The reflections from the film and substrate were observed at nearly identical Q_x and that from the film was not located at reciprocal vectors estimated from lattice parameters of bulk.[18] This analysis indicates that the β-$(Al_{0.28}Ga_{0.72})_2O_3$ film is under tensile strain. It should be

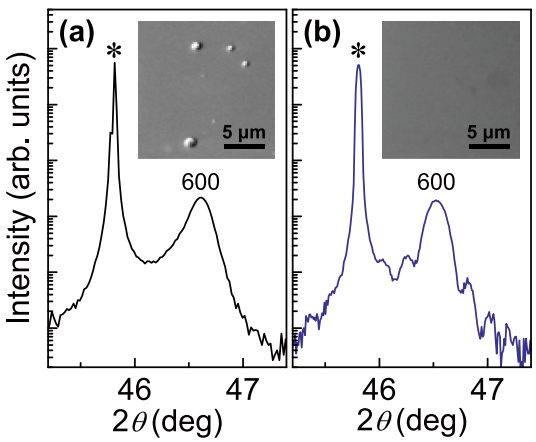

FIG. 1. Out-of-plane XRD patterns for the 50-nm-thick β-$(Al_{0.2}Ga_{0.8})_2O_3$ films grown by (a) continuous laser ablation of a sintered $(Al_{0.2}Ga_{0.8})_2O_3$ tablet and (b) repeating alternative laser ablation of β-Ga_2O_3 and α-Al_2O_3 single crystals. The reflections labeled by the asterisk (*) come from β-Ga_2O_3 (100) substrates. The insets show SEM images of the same samples.

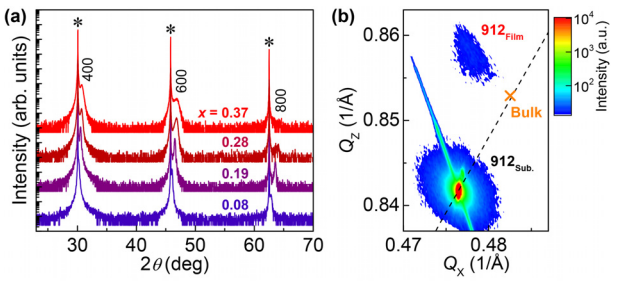

FIG. 2. (a) Out-of-plane XRD patterns for 50-nm-thick β-$(Al_xGa_{1-x})_2O_3$ films ($x = 0.08$, 0.19, 0.28, and 0.37). The reflections labeled by the asterisks (*) come from β-Ga_2O_3 (100) substrates. (b) Reciprocal space map around 912 reflection of the β-$(Al_{0.28}Ga_{0.72})_2O_3$ film. Reciprocal vectors of Q_X and Q_Z correspond to real-space vectors normal to (012) and (100) planes, respectively. The crossing bar indicates the position of β-$(Al_xGa_{1-x})_2O_3$ 912 reflection, estimated from lattice parameters of bulk. The dashed line intersects the origin and 912 reflection from the substrate.

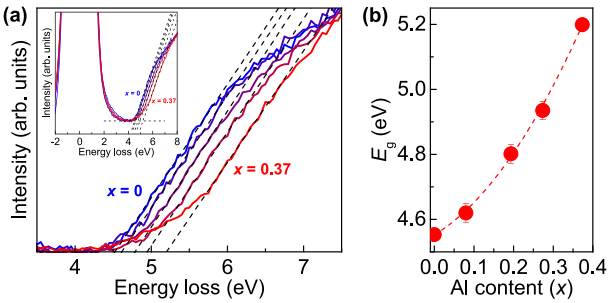

FIG. 3. (a) REELS spectra near onsets of loss spectra for β-$(Al_xGa_{1-x})_2O_3$ films [$x = 0$, 0.08, 0.19, 0.27, and 0.37 (from left to right)]. The intercepts of dashed lines correspond to E_g. The inset shows the wide-range REELS spectra. The zero-loss peaks are set to 0 eV for all samples. (b) Al content (x) dependence of E_g estimated from the REELS spectra. Error bars represent the standard errors for a number of measurements.

noted that the film reflection has a tail toward the position of bulk, implying the upper bound of the Al content for coherent epitaxy of the 50-nm-thick film. Indeed, for the higher-x β-$(Al_{0.37}Ga_{0.63})_2O_3$ film, the $h00$ peak positions ($h = 4$, 6, and 8) in the out-of-plane XRD pattern [Fig. 2(a)] considerably shifted to a lower angle side. This shift indicated the lattice relaxation of the β-$(Al_{0.37}Ga_{0.63})_2O_3$ film from the substrate.

Next, we investigated the band structures of β-$(Al_xGa_{1-x})_2O_3$ films. Figure 3(a) shows the REELS spectra of the β-$(Al_xGa_{1-x})_2O_3$ films. All the loss spectra clearly indicated linear slope regions, which gradually shifted to higher loss energy with the increasing Al content. The E_g values were defined to be loss energy at intercepts between linear fits to flat and slope regions (see the inset). Figure 3(b) shows the obtained E_g as a function of the Al content. The E_g of the β-$(Al_xGa_{1-x})_2O_3$ films systematically increased from 4.55 ± 0.01 eV ($x = 0$) to 5.20 ± 0.02 eV ($x = 0.37$).

It is notable that our analysis captures a bowing behavior. Krueger reported a linear x-dependence of E_g for β-$(Al_xGa_{1-x})_2O_3$, as expressed by $4.75 + 1.87x$.[18] Their data are based on XPS analyses for polycrystalline samples and thus can be considered as an *averaged* standard. Compared with those in a range of $x = 0$–0.37 ($E_g = 4.75$–5.44 eV), E_g we estimated is considerably narrower, which can be ascribed not only to the bowing but also a number of factors. First, the variation of E_g intrinsic to the β-gallia structure ($C2/m$) depends on the measurement technique and geometry. Our REELS data were taken for the (100) plane with a detection angle set to ~30° off from the surface normal. In this geometry, the spectra reflect an anisotropic band profile but neither just average nor specific to a basal plane.[2] Second, the effect of stain on modulation of the band structure should be considered because we observed tensile strain in the plane and its relaxation tendency with increasing x, as described already. The residual compressive strain along the out-of-plane may give rise to narrowing E_g, which would lead to the observed bowing behavior. In this vein, our original data are useful for β-Ga_2O_3 based (100) heterojunctions.

We determined the band alignment at the β-$(Al_xGa_{1-x})_2O_3/\beta$-$Ga_2O_3$ interface by a standard procedure using XPS.[3,22] We prepared three kinds of samples to suppose actual β-Ga_2O_3-based device structures: (a) 170-nm-thick β-Ga_2O_3 homoepitaxial film, (b) 50-nm-thick β-$(Al_xGa_{1-x})_2O_3$ films grown on β-Ga_2O_3 substrates, and (c) 2-nm-thick β-Ga_2O_3 films grown on (b). Photoemission spectra independently obtained from the samples were analyzed as follows: The peak positions of Al $2p$ and Ga $3p_{3/2}$ core levels were determined by fitting using a Gaussian function, while energy levels of valence-band maximum (VBM) were estimated by the linear extrapolation of the edge. The errors of core levels and VBM were less than 10 meV and 50 meV, respectively. The obtained binding energies are summarized in Table I. We extracted discontinuities of conduction-band minima and valence-band maxima from the following equations, respectively:

$$\Delta E_V = \left(E^{Ga_2O_3}_{Ga\,3p_{3/2}} - E^{Ga_2O_3}_{VBM}\right) - \left(E^{(Al_xGa_{1-x})_2O_3}_{Al\,2p} - E^{(Al_xGa_{1-x})_2O_3}_{VBM}\right) - \left(E^{Interface}_{Ga\,3p_{3/2}} - E^{Interface}_{Al\,2p}\right),$$

and

$$\Delta E_C = \left(E^{(Al_xGa_{1-x})_2O_3}_{g}\right) - \left(E^{Ga_2O_3}_{g}\right) - \Delta E_V,$$

where $E^{Ga_2O_3}_{Ga\,3p_{3/2}}$ and $E^{Ga_2O_3}_{VBM}$ are the peak positions of the Ga $3p_{3/2}$ core level and VBM for β-Ga_2O_3, respectively, $E^{(Al_xGa_{1-x})_2O_3}_{Al\,2p}$ and $E^{(Al_xGa_{1-x})_2O_3}_{VBM}$ are the peak positions of Al $2p$ core levels and VBM for β-$(Al_xGa_{1-x})_2O_3$, respectively, $E^{Interface}_{Ga\,3p_{3/2}}$ and $E^{Interface}_{Al\,2p}$ are the peak positions of Ga $3p_{3/2}$ and Al $2p$ core levels at the interface, respectively, and $E^{(Al_xGa_{1-x})_2O_3}_{g}$ and $E^{Ga_2O_3}_{g}$ are E_g of β-$(Al_xGa_{1-x})_2O_3$ and β-Ga_2O_3 determined from the REELS measurement, respectively. The sample (c) was designed by taking the escape depth of photoelectrons under our measurement condition into account, so that the Ga $3p_{3/2}$ and Al $2p$ peaks could be identified as those from the top β-Ga_2O_3 film and buried β-$(Al_xGa_{1-x})_2O_3$ film, respectively. See supplementary material for details (Fig. S2). In this geometry, the top β-Ga_2O_3 film is under constraint of strain, and our analysis also requires the Ga $3p_{3/2}$ peak from the unstrained sample (a). Therefore, any effect arising from strain would be involved for determination of the band alignment. We tentatively assumed the identical electronic structure for β-Ga_2O_3 films between samples (a) and (c).

Having established the values of ΔE_C and ΔE_V, we illustrated the band alignment at the β-$(Al_xGa_{1-x})_2O_3/\beta$-$Ga_2O_3$ interface (Fig. 4). The ΔE_C and ΔE_V values of $x = 0.37$ ($x = 0.27$) were 0.52 ± 0.08 eV (0.37 ± 0.08 eV) and

TABLE I. The summary of the Al content, E_g, and energy differences of core levels estimated from AES, REELS, and XPS, respectively.

Al content	E_g (eV)	$E^{Ga_2O_3}_{Ga\,3p_{3/2}} - E^{Ga_2O_3}_{VBM}$ (eV)	$E^{(Al_xGa_{1-x})_2O_3}_{Al\,2p} - E^{(Al_xGa_{1-x})_2O_3}_{VBM}$ (eV)	$E^{Interface}_{Ga\,3p_{3/2}} - E^{Interface}_{Al\,2p}$ (eV)
0	4.55 ± 0.01	102.14 ± 0.05		
0.27	4.94 ± 0.03		70.90 ± 0.05	31.22 ± 0.01
0.37	5.20 ± 0.02		70.88 ± 0.05	31.13 ± 0.01

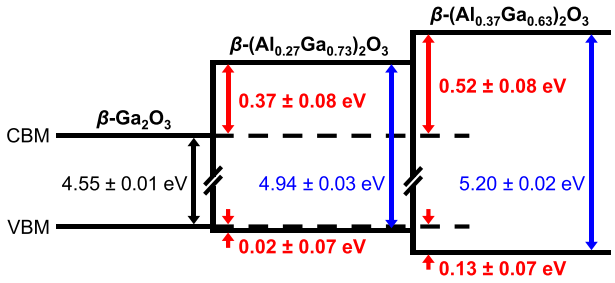

FIG. 4. Band alignments at (100) interfaces between β-$(Al_xGa_{1-x})_2O_3$ and β-Ga_2O_3. The CBM and VBM denote the conduction-band minimum and valence-band maximum, respectively.

0.13 ± 0.07 eV (0.02 ± 0.07 eV), respectively. Note that the errors were defined as the root-mean-square errors, where the errors estimated in XPS and REELS measurements were included (see Table I). This band alignment can be characterized as type-I within the limit of accuracy in each electron spectroscopy. Moreover, substantially large ΔE_C is experimentally identified, which provides valuable information for designing heterojunction devices.

As shown in Fig. 4, ΔE_C predominantly increases with alloying Al_2O_3, while ΔE_V almost remains intact, which is different from Al/Ga based III-V compound semiconductors [i.e., ΔE_C:$\Delta E_V = 65$:35 of (Al,Ga)As/GaAs and ΔE_C:$\Delta E_V = 2$:1 of (Al,Ga)N/GaN systems].[27,28] This difference arises from different nature of chemical bonding. Compared to arsenides and nitrides, oxides have strong ionic bonding. In the case of β-$(Al_xGa_{1-x})_2O_3$, conduction and valence bands are composed mostly of Al/Ga *s* and O 2*p* states, respectively, as estimated from first-principles calculations and indicated in α-phase systems.[29,30] Therefore, contribution of the cation-site substitution dominantly appears in the conduction band. Large ΔE_C is the advantage for the formation of 2DEG and HFET operations, enabling refinement of modulation doping structures as demonstrated in (Al,Ga)As and (Al,Ga)N systems.[27,31–33]

In conclusion, we fabricated high quality β-$(Al_xGa_{1-x})_2O_3$ films on β-Ga_2O_3 (100) substrates by using PLD and revealed the band alignment at β-$(Al_xGa_{1-x})_2O_3$/β-Ga_2O_3 interfaces with using REELS and XPS. The crystallinity and surface flatness of the films was substantially improved using the repeating alternate target ablation technique. E_g as a function of the Al content indicated the bowing behavior. The band alignment of the present system was found to be type-I, where the ΔE_C and ΔE_V values of $x = 0.37$ ($x = 0.27$) were 0.52 ± 0.08 eV (0.37 ± 0.08 eV) and 0.13 ± 0.07 eV (0.02 ± 0.07 eV), respectively. Our study provides a better understanding of how the β-$(Al_xGa_{1-x})_2O_3$/β-Ga_2O_3 heterojunction is designed and fabricated for device applications.

See supplementary material for AFM images of the β-Ga_2O_3 substrate and β-$(Al_xGa_{1-x})_2O_3$ films and XPS spectra for determining the band alignment at the β-$(Al_xGa_{1-x})_2O_3$/β-Ga_2O_3 interfaces.

The authors thank M. Tada of the Center for advanced Materials Analysis for assistance with AES and REELS measurements. This work was partly supported by MEXT Element Strategy Initiative to Form Core Research Center and a Grant-in-Aid for Scientific Research (Nos. 15H03881 and 16J09832) from the Japan Society for the Promotion of Science Foundation. R.W. acknowledges the financial support from JSPS.

[1]R. Roy, V. G. Hill, and E. F. Osborn, J. Am. Chem. Soc. **74**, 719 (1952).
[2]T. Onuma, S. Saito, K. Sasaki, T. Masui, T. Yamaguchi, T. Honda, and M. Higashiwaki, Jpn. J. Appl. Phys., Part 1 **54**, 112601 (2015).
[3]M. Hattori, T. Oshima, R. Wakabayashi, K. Yoshimatsu, K. Sasaki, T. Masui, A. Kuramata, S. Yamakoshi, K. Horiba, H. Kumigashira, and A. Ohtomo, Jpn. J. Appl. Phys., Part 1 **55**, 1202B6 (2016).
[4]M. Higashiwaki, K. Sasaki, A. Kuramata, T. Masui, and S. Yamakoshi, Appl. Phys. Lett. **100**, 013504 (2012).
[5]E. G. Víllora, K. Shimamura, Y. Yoshikawa, T. Ujiie, and K. Aoki, Appl. Phys. Lett. **92**, 202120 (2008).
[6]K. Sasaki, A. Kuramata, T. Masui, E. G. Víllora, K. Shimamura, and S. Yamakoshi, Appl. Phys. Express **5**, 035502 (2012).
[7]A. Kuramata, K. Koshi, S. Watanabe, Y. Yamaoka, T. Masui, and S. Yamakoshi, Jpn. J. Appl. Phys., Part 1 **55**, 1202A2 (2016).
[8]R. Wakabayashi, K. Yoshimatsu, M. Hattori, and A. Ohtomo, Appl. Phys. Lett. **111**, 162101 (2017).
[9]E. Ahmadi, O. S. Koksaldi, X. Zheng, T. Mates, Y. Oshima, U. K. Mishra, and J. S. Speck, Appl. Phys. Express **10**, 071101 (2017).
[10]M. Higashiwaki, K. Sasaki, T. Kamimura, M. H. Wong, D. Krishnamurthy, A. Kuramata, T. Masui, and S. Yamakoshi, Appl. Phys. Lett. **103**, 123511 (2013).
[11]E. G. Villora, K. Shimamura, Y. Yoshikawa, K. Aoki, and N. Ichinose, J. Cryst. Growth **270**, 420 (2004).
[12]Z. Galazka, K. Irmscher, R. Uecker, R. Bertram, M. Pietsch, A. Kwasniewski, M. Naumann, T. Schulz, R. Schewski, D. Klimm, and M. Bickermann, J. Cryst. Growth **404**, 184 (2014).
[13]K. Hoshikawa, E. Ohba, T. Kobayashi, J. Yanagisawa, C. Miyagawa, and Y. Nakamura, J. Cryst. Growth **447**, 36 (2016).
[14]M. Higashiwaki, A. Kuramata, H. Murakami, and Y. Kumagai, J. Phys. D: Appl. Phys. **50**, 333002 (2017).
[15]M. Higashiwaki, K. Konishi, K. Sasaki, K. Goto, K. Nomura, Q. T. Thieu, R. Togashi, H. Murakami, Y. Kumagai, B. Monemar, A. Koukitu, A. Kuramata, and S. Yamakoshi, Appl. Phys. Lett. **108**, 133503 (2016).
[16]A. J. Green, K. D. Chabak, E. R. Heller, R. C. Fitch, M. Baldini, A. Fiedler, K. Irmscher, G. Wagner, Z. Galazka, S. E. Tetlak, A. Crespo, K. Leedy, and G. H. Jessen, IEEE Electron Device Lett. **37**, 902 (2016).
[17]M. Higashiwaki, H. Murakami, Y. Kumagai, and A. Kuramata, Jpn. J. Appl. Phys., Part 1 **55**, 1202A1 (2016).
[18]B. W. Krueger, C. S. Dandeneau, E. M. Nelson, S. T. Dunham, F. S. Ohuchi, and M. A. Olmstead, J. Am. Ceram. Soc. **99**, 2467 (2016).
[19]T. Oshima, Y. Kato, N. Kawano, A. Kuramata, S. Yamakoshi, S. Fujita, T. Oishi, and M. Kasu, Appl. Phys. Express **10**, 035701 (2017).
[20]S. Krishnamoorthy, Z. Xia, C. Joishi, Y. Zhang, J. Mcglone, J. Johnson, M. Brenner, A. R. Arehart, J. Hwang, S. Lodha, and S. Rajan, Appl. Phys. Lett. **111**, 23502 (2017).
[21]K. Konishi, T. Kamimura, M. H. Wong, K. Sasaki, A. Kuramata, S. Yamakoshi, and M. Higashiwaki, Phys. Status Solidi **253**, 623 (2016).
[22]E. A. Kraut, R. W. Grant, J. R. Waldrop, and S. P. Kowalczyk, Phys. Rev. Lett. **44**, 1620 (1980).
[23]R. Wakabayashi, T. Oshima, M. Hattori, K. Sasaki, T. Masui, A. Kuramata, S. Yamakoshi, K. Yoshimatsu, and A. Ohtomo, J. Cryst. Growth **424**, 77 (2015).
[24]T. Fukumura, M. Ohtani, M. Kawasaki, Y. Okimoto, T. Kageyama, T. Koida, T. Hasegawa, and Y. Tokura, Appl. Phys. Lett. **77**, 3426 (2000).
[25]H. Mashiko, T. Oshima, and A. Ohtomo, Jpn. J. Appl. Phys., Part 1 **51**, 11PG11 (2012).
[26]W. K. A. Kumuduni, Y. Nakata, Y. Sasaki, T. Okada, M. Maeda, T. Kisu, M. Takeo, and K. Enpuku, J. Appl. Phys. **77**, 5961 (1995).
[27]J. Batey and S. L. Wright, J. Appl. Phys. **59**, 200 (1986).
[28]P. Reddy, I. Bryan, Z. Bryan, J. Tweedie, S. Washiyama, R. Kirste, S. Mita, R. Collazo, and Z. Sitar, Appl. Phys. Lett. **107**, 91603 (2015).
[29]K. Yamaguchi, Solid State Commun. **131**, 739 (2004).
[30]T. Uchida, R. Jinno, S. Takemoto, K. Kaneko, and S. Fujita, Jpn. J. Appl. Phys., Part 1 **57**, 40314 (2018).
[31]M. Kuroda, H. Ishida, T. Ueda, and T. Tanaka, J. Appl. Phys. **102**, 93703 (2007).
[32]T. Mimura, S. Hiyamizu, T. Fujii, and K. Nanbu, Jpn. J. Appl. Phys., Part 2 **19**, L225 (1980).
[33]M. O. Watanabe, J. Yoshida, M. Mashita, T. Nakanisi, and A. Hojo, J. Appl. Phys. **57**, 5340 (1985).